RSC Advances

PAPER

View Article Online
View Journal | View Issue

Cite this: *RSC Adv.*, 2025, **15**, 29053

Tuning the spontaneous emission of CdTe quantum dots with hybrid silicon–gold nanogaps

Areeg Al-hamadani,[ab] Ali Al-Dulami,[ab] Theresa Bartschmid,[c] Johannes Menath,[d] Alina Muravitskaya,[a] Nicolas Vogel,[d] Gilles R. Bourret,[c] Jean-Sebastien G. Bouillard *[a] and Ali M. Adawi *[ae]

Hybrid dielectric–metal nanogaps offer unique properties such as enhanced local density of optical states (LDOS) and simultaneously high quantum yield and coupling efficiency, with applications in bright single-photon sources, efficient nanoLEDs and imaging spectroscopy. In this work we report on silicon–gold hybrid nanogaps, considering both silicon nanorods on a gold film and gold nanorods on a silicon surface and compare them to their purely metallic and dielectric equivalent. To obtain the necessary nanometer-scale control, a combination of colloidal lithography, metal assisted chemical etching (MACE), and layer-by-layer polyelectrolyte approach were used to construct the nanogaps. Quantum emitters were incorporated in the nanogap in the form of a CdTe quantum dot monolayer. The efficient coupling between the quantum dot monolayer and the nanogap modes results in hybrid nanogaps outperforming their homogeneous counterpart, with the gold nanorod–silicon hybrid nanogap offering the largest emission rate enhancement factor of 51. Specifically, Purcell enhancements were increased by a factor of ~2 for silicon nanorod–gold film and ~1.5 for gold nanorod–silicon surface nanogaps compared to purely dielectric and metallic geometries respectively. These results, supported by FDTD simulations, highlight hybrid nanogaps as cornerstones for probing light–matter-interactions under extreme optical confinement with applications such as low cost and low power consumption ultrafast LEDs for short distance on-chip and chip-to-chip communications.

Received 27th June 2025
Accepted 6th August 2025

DOI: 10.1039/d5ra04583e

rsc.li/rsc-advances

Introduction

Spontaneous emission of quantum emitters, such as quantum dots[1] or fluorophores,[2] is a fundamental optical process that plays a pivotal part in a wide range of applications[3] including lasers,[4,5] optical interconnection,[6–8] fast-LEDs for short range on chip or chip-to-chip data communications,[7,9] single photon sources for quantum cryptography[10,11] and imaging spectroscopy.[9,12] However, to fulfil these applications, it is crucial to both enhance the spontaneous emission rate of quantum emitters over a large bandwidth while retaining a high quantum yield,[7] and to achieve control over emission directionality in order to ensure high collection efficiency and optimum use of the emitted light.[13] Consequently, this requires the development of optical resonators with increased local density of optical states (LDOS), low optical loss, and optical mode confinement well below the diffraction limit.[14,15] Three types of optical resonators can be used to control the spontaneous emission: (i) Photonic crystal nanocavities,[16,17] which are characterised by low optical losses, but very narrow bandwidth and poor light coupling efficiency.[18] (ii) All-metal plasmonic nanogaps[19,20] which provide highly increased LDOS,[13,15,19,21] high collection efficiency,[14] but suffer from high optical losses.[15,22] (iii) All dielectric nanogaps, based on high refractive index materials,[23–30] which offer low to no optical loss but result in modest increase in LDOS combined with good coupling efficiency.[23,25,27] By coupling a high refractive index dielectric nanostructure to a plasmonic nanostructure[31–34] it is possible to enhance the LDOS while maintaining low optical losses.[22,35–43] A range of hybrid dielectric–plasmonic nanogaps has already been investigated, including the coupling between a dielectric nanosphere and a plasmonic nanoparticle,[36] a dielectric nanosphere coupled to a continuous gold film[22,37] and dielectric nanowires coupled to a metallic film.[33,35,38,44] Silicon nanosphere coupled to a gold film have been reported to offer photoluminescence enhancements up to 786 (ref. 37) and Purcell factors up to 42.[22] On the other hand, Silicon nanowires coupled to a gold film have provided up to 10 times photoluminescence intensity enhancements,[35] while

[a]*Department of Physics, University of Hull, Cottingham Road, HU6 7RX, UK. E-mail: a.adawi@hull.ac.uk; j.bouillard@hull.ac.uk*

[b]*Department of Physics, College of Science, University of Diyala, Baquba City 32001, Diyala Governorate, Iraq*

[c]*Department of Chemistry and Physics of Materials, University of Salzburg, A-5020 Salzburg, Austria*

[d]*Friedrich-Alexander-Universität Erlangen-Nürnberg (FAU), Institute of Interfaces and Particle Technology, 91058 Erlangen, Germany*

[e]*Department of Physics, School of Science, The University of Jordan, Amman 11942, Jordan*

nanogaps based on a ZnO nanowire coupled to a silver metallic film have demonstrated Purcell factors of 60 combined with 5 folds photoluminescence intensity enhancements.[38]

However, despite the enormous potential of hybrid dielectric–plasmonic nanogaps, the coupling of low aspect ratio dielectric rods, AR $\leq$ 10, with a metallic film has not been investigated, with most studies focussing on nanowires with aspect ratio in the range of 40 to 115. While high aspect ratio nanorods behave as waveguides making them more suited for applications requiring in-plane coupling,[38] low aspect ratio nanorods offer high out-of-plane coupling efficiency. Furthermore, the coupling between plasmonic nanorods and a high refractive index substrate such as silicon or between silicon nanorods and a silicon surface have, to date, been rarely studied.[45]

In this work, we address this gap in knowledge by exploring hybrid plasmonic–dielectric nanogaps in a previously unstudied region of the parameter space. We systematically investigate and compare the emission rate enhancements and photoluminescence intensity enhancements in four different nanogap geometries formed between either silicon nanorods or gold nanorods and either a gold film or a silicon surface (see Fig. 1). It is well-known that the nanogap properties are strongly dependent on the gap dimensions. To directly compare the four distinct geometries, the reproducibility of the nanogap thickness is essential. Here, polyelectrolyte layer-by-layer deposition[46] combined with a QD monolayer was used to provide nanometre control over the gap sizes, therefore enabling direct comparison between the various geometries. Additionally, whereas gold nanorods (AuNRs) are readily obtainable commercially, high refractive index nanoparticles can be challenging to synthesise. In this work, highly crystalline silicon nanorods (SiNRs) were fabricated using a combination of colloidal lithography[47] and metal-assisted chemical etching[48] (MACE), before being removed from the substrate and suspended in a solution. Both experimental results and full wave FDTD simulations show that all four nanogap geometries provide high emission rate enhancements combined with high coupling efficiency over the visible and near infrared spectral region. However, the hybrid plasmonic–dielectric nanogaps displayed overall superior performances compared to all-metal or all-dielectric nanogap geometries.

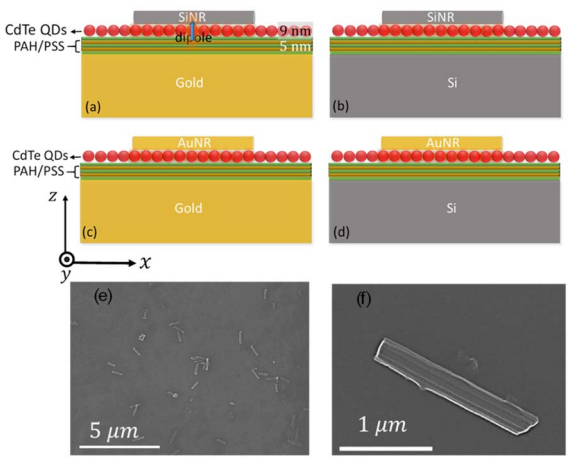

Fig. 1 (a–d) Schematic representations of the nanogaps investigated in this study. (e) and (f) SEM images of the SiNRs recorded at two different magnifications.

Experimental section

FDTD calculations

Ansys Lumerical FDTD was used to calculate emission rate enhancements. In all simulations, the emitter was modelled as a classical dipole polarized along the *z*-direction (perpendicular to the gold film/silicon surface, see Fig. 1) and located in a 14 nm gap at the centre of the QD monolayer (see Fig. 1a). The enhancements in the emission decay rates were calculated using $\frac{\Gamma_T}{\Gamma_0} = \frac{P_T}{P_0}$ and $\frac{\Gamma_{Rad}}{\Gamma_0} = \frac{P_{Rad}}{P_0}$, where Γ_0 is the dipole decay rate in free space, Γ_T is the total decay rate, Γ_{Rad} is the radiative decay rate, P_0 is the dipole radiated power in free space, P_r is the total power dissipated by the dipole in the presence of the nanogap, and P_{Rad} is the radiated power by the dipole. The nanogap region was modelled as a homogeneous non-dispersive region of refractive index 1.5 corresponding to the average refractive index of the QD layer and the polyelectrolyte multilayer. Experimental data from Johnson and Christy[49] and Palik[50] were used to describe the dielectric function of gold and silicon respectively. In our calculations we employed a 1 nm grid spacing and perfect matching layer boundary conditions. Calculations were terminated when the fields reached 10^{-7} of their initial value.

Silicon nanorods fabrication

Silicon nanorod (SiNR) solutions were prepared *via* a combination of colloidal lithography, metal assisted chemical etching (MACE), and subsequent removal from the substrate, as previously described.[51–57] The combination of colloidal lithography and MACE is a versatile approach to synthesise SiNRs of diameters from 100 nm up to several microns with length from 400 nm to few microns on a wafer scale. A colloidal solution of SiO_2@PNiPAm core–shell nanoparticles (NPs) was prepared following a modified Stöber process, and a subsequent polymerization of PNIPAm (poly(*N*-isopropylacrylamide)). The soft PNIPAm shell acts as a spacer to separate the silica cores,[58] ensuring well-separated nanorods after the MACE process. The colloidal particles were self-assembled as a monolayer on the air–water interface using a Langmuir–Blodgett trough and transferred to a pre-cleaned Si wafer.[57,59] The polymer–shell of the assembled core–shell NPs was removed by oxygen plasma (Quorum Emitech K1050X) for 12 min at 50 W with an oxygen flow rate of 20 mL min^{-1}. Subsequently, a layer of aluminum-doped zinc oxide (AZO) was sputtered (Clustex 100 M sputtering system by Leybold Optics, 75 W, 1 s), followed by an Au sputtering step for 200 s at 40 mA (Cressington Sputter Coater 108 auto). The SiO_2 spheres were removed using adhesive tape (Scotch magic tape) followed by a short oxygen plasma cleaning step for 5 min at 50 W with a flow rate of 20 mL min^{-1} to remove

traces of the deposited adhesive. Next, the sample was immersed in an aqueous solution of H_2O_2 and HF (10 mL H_2O, 0.75 mL H_2O_2, 10 mL HF) for 2 min, a process known as metal-assisted chemical etching[48] (MACE). In this step, vertically aligned silicon rods form due to preferential oxidation and dissolution of Si in proximity of the Au film, which sinks into the Si substrate during this process. The synthesis of the SiNR array (see Fig. S1b) was finished with an after-treatment in an aqueous solution of HF (20 mL H_2O, 4 mL HF) for 5 min to remove any residual porous SiO_2 that formed during MACE. The templated Au film at the bottom of the SiNR array was dissolved in aqueous KI/I_2 solution (10 g KI and 5 g I_2 dissolved in 85 g H_2O) for 80 min, followed by two rinsing steps in deionized water and one rinsing step in ethanol.[51–55]

In order to transfer the SiNRs into solution, they were scratched from the surface with a tweezer and transferred to 250 μL of absolute ethanol. Additionally, the entire Si piece was sonicated for 15 min in absolute ethanol to break the remaining SiNRs off the Si substrate.[60] The final SiNRs have a diameter ~140 nm and length of 1000 nm (see Fig. 1e, f and S1).

Nanogap fabrication

The nanogaps in this study are based on the coupling of a silicon nanorod (SiNR) or a gold nanorod (AuNRs) with either a 100 nm thick gold film or a Si surface. The AuNRs measured 100 nm in diameter, 1000 nm in length and were purchased from Nanopartz, whereas the SiNRs were synthesized as described above. In all the investigated structures, the nanogap width was fixed at 13.6 nm, using a spacer composed of polyelectrolyte layers combined with a monolayer of colloidal quantum dots. Si substrates were coated with a 100 nm-thick gold layer thermally evaporated (Auto 500, HHV) through a shadow mask, allowing for the fabrication of nanorod-gold and nanorod-Si nanogaps simultaneously (see Fig. 1a to d).

The thermal evaporation was followed by 2.5 pairs of PAH–PSS polyelectrolyte spacer layers.[13,61] The PAH–PSS polyelectrolyte spacer layers were formed using layer-by-layer dip-coating technique. Firstly, the substrate was O_2 plasma treated at 100 W and 0.27 mbar for 5 seconds, then dipped in an aqueous mixture of 5.28 μM of poly(allylamine) hydrochloride (PAH Sigma-Aldrich) with 0.248 M of NaCl (Sigma-Aldrich) for 5 min. Then the substrate was washed in deionized water and dried using nitrogen gas to obtain 1 nm layer of PAH. Next, the substrate was immersed in an aqueous solution of 44.4 μM of polystyrene sulfonate (PSS, Sigma-Aldrich) and 0.248 M NaCl for 5 minutes, then washed in deionized water and dried using nitrogen gas to form 1 nm PSS layer. This process results in a highly reproducible and controllable spacer layer with a total thickness of 5 nm.

As the active layer, colloidal quantum dots were chosen for their high stability and use in display technology.[62] A monolayer of CdTe QDS (8.6 nm in diameter from Plasma Chem) was subsequently deposited using dip-coating, by immersing the sample in a 1 g per L CdTe QDs aqueous solution for 5 min, followed by drying using nitrogen gas. Zeta potential measurements (Fig. S2) showed that the CdTe QDs are negatively charged. This approach provides a uniform monolayer of CdTe QDs (see Fig. S1a).

To complete the nanogaps, the SiNRs or AuNRs were spin-coated at a speed of 2000 rpm for 60 seconds onto the CdTe QD monolayer surface.

Scattering measurements

Dark field scattering[63] measurements were performed by illuminating the nanogap with collimated white light at an angle of 60° relative to the sample normal using a 10× long working distance Mitutoyo objective lens of numerical aperture 0.28. The scattered light was collected at normal incidence using a 50× long working distance Mitutoyo objective lens of numerical aperture 0.55. The scattered light was then directed toward an iHR320 Horiba spectrometer equipped with a 150 lines per mm grating and a liquid nitrogen cooled Symphony CCD. Fig. S3 shows typical dark-field images of the fabricated nanogaps.

CW and time-resolved photoluminescence measurements

The CW and time-resolved photoluminescence measurements were carried out using a 405 nm pulsed diode laser with 40 ps width and 20 MHz repetition rate. The nanogap was excited using the 405 nm laser diode *via* a 100× Olympus objective lens of numerical aperture 0.9, providing an excitation area of ~1 micron in diameter. The same objective was used to collect the photoluminescence signal, which was spectrally resolved using a MicroHR Horiba spectrometer with a 150 lines per mm grating and then directed towards either a ProEM Princeton Instruments CCD for CW photoluminescence measurements or a Becker and Hickl HPM-100 detector for photoluminescence time-resolved measurements. The nanogap photoluminescence decay rate was extracted *via* fitting a double-exponential model,[64] $I(t) = a_1 e^{-\Gamma_1 t} + a_2 e^{-\Gamma_2 t}$, after deconvolution of the instrument response function (IRF). The fast decay rate component, Γ_1, is attributed to the coupling between the quantum dot dipoles and the confined electromagnetic field of the nanogap.[21,65,66]

Results and discussion

Four different nanogap geometries were considered (Fig. 1) and directly compared: a purely dielectric structure consisting of silicon nanorod coupled to a silicon surface (SiNR–Si), a purely plasmonic structure composed of a gold nanorod coupled to a gold film (AuNR–Au), and two hybrid structures formed of a silicon nanorod on a gold film (SiNR–Au) or a gold nanorod on a silicon surface (AuNR–Si).

Modelling emission rate enhancements

In a first instance, the potential of each geometry to modify emission processes was numerically investigated. In the simulations, the ideal case was considered, where the QDs emitting monolayer is represented by a single dipole polarised along the *z*-axis and located at the centre of the QD monolayer (Fig. 2).

The hybrid SiNR–Au nanogap (Fig. 2a and b) displays moderate emission decay rate enhancements, with a maximum enhancement of ~200 times, over a wide spectral range covering both the visible and near infrared. This enhancement is associated with a high quantum yield (0.5–0.90). On the other hand, the all dielectric SiNR–Si nanogap (Fig. 2c and d) exhibits lower emission enhancements than the hybrid gaps, with a maximum enhancement of ~45 times. These results are in line with the electric field distribution inside the nanogap, where the emission rate is proportional to the imaginary part of the electric field at the dipole location,[67] $\Gamma \propto \mathrm{Im}(E(r_0))$ (see Fig. S4). However, this structure provides a consistently high quantum yield, above 0.75, across the whole 600–1800 nm wavelength range. Both nanogaps offer a relatively directional emission profile confined around $\theta = 40°$ with angular width of 10° relative to the normal (see inset of Fig. 2d and S5).

In comparison, the nanogaps based on a gold nanorod offer greatly enhanced emission rates. The purely plasmonic nanogap (Fig. 2e and f) is associated with the highest emission rate enhancements, up to 2000 times. However, this high enhancement is associated with correspondingly high non-radiative losses, leading to a quantum yield consistently below 0.36 (Fig. 2f). The hybrid geometry, AuNR–Si, provides moderate decay rate enhancements, peaking at ~400 times, albeit with an overall higher quantum yield in the range 0.45–0.82. Interestingly, both AuNR–Au and AuNR–Si result in the similar directional emission profile around $\theta = 45° \pm 10°$(see Fig. 2h and S6) as the silicon nanorod based structures. However, the structures based on the gold nanorod emission exhibit an additional emission directionality around $\theta = 15° \pm 10°$.

The nanogap modes can be further controlled *via* the gold or silicon film thickness.[68–71] Decreasing the gold film thickness down to 10 nm leads to a broadening and red-shift of the nanogap modes[68] coupled to a reduction of their quantum efficiency (Fig. S7). Similarly, reducing the silicon film thickness to 10 nm leads to a lower quantum efficiency (Fig. S8). Consequently, both the silicon and gold film thickness can be used to control the spectral position and *Q*-factor of the gap modes (Fig. S7 and S8) for increased tunability. The spectral response of the nanogap can be further tuned by changing the gap size and nanorod geometrical parameters.

The FDTD calculations clearly indicate the potential of hybrid dielectric–metallic nanogaps to shape the spontaneous emission process of a layer of quantum dots deposited within these gaps.

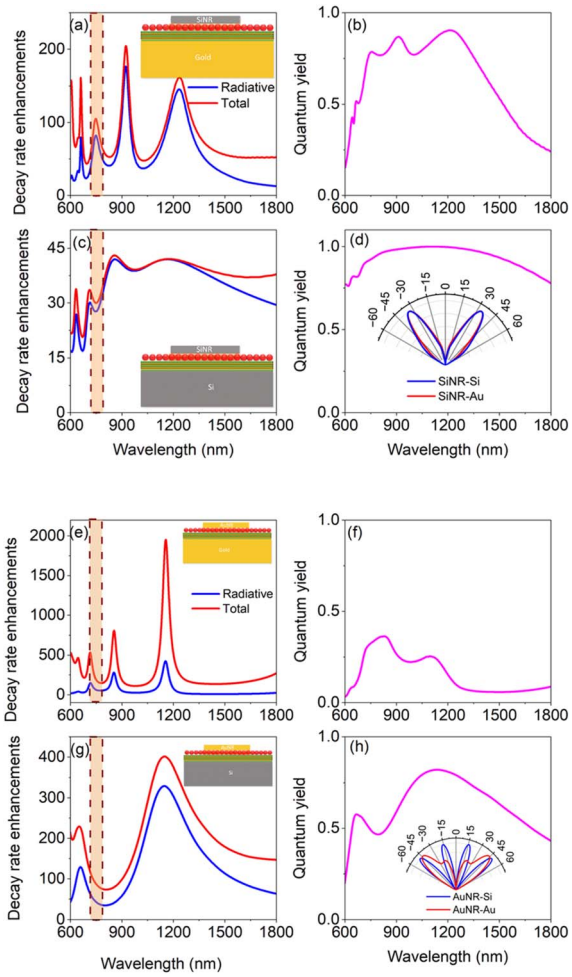

Fig. 2 (a) Calculated emission rate enhancements from a SiNR–Au nanogap. (b) Calculated quantum efficiency of SiNR–Au nanogap. (c) Calculated emission rate enhancements from a SiNR–Si nanogap. (d) Calculated quantum efficiency of SiNR–Si nanogap. The inset shows the emission profile of SiNR–Au and SiNR–Si nanogaps at $\lambda = 750$ nm. (e) Calculated emission rate enhancements from an AuNR–Au nanogap. (f) Calculated quantum efficiency of AuNR–Au nanogap. (g) Calculated emission rate enhancements from a AuNR–Si nanogap. (h) Calculated quantum efficiency of AuNR–Si nanogap. The inset shows the emission profile of SiNR–Au and SiNR–Si nanogaps at $\lambda = 750$ nm. The shaded region in parts (a), (c), (e) and (g) represents the spectral bandwidth of the used QDs in this work.

Experimental verification of emission rate enhancement

Samples containing the four nanogap geometries were fabricated following the procedure described in the experimental section, ensuring the highly reproducible nanogap dimensions and high SiNR crystallinity necessary for a reliable comparison between all four geometries. The typical scattering spectra of all fabricated nanogaps spectrally overlap with the emission spectrum of the CdTe QD monolayer (Fig. 3), suggesting that the nanogaps can modify the QD emission process.

As can be seen from Fig. 4, S6 and Table S1, the emission decay curve of the QD monolayer on a glass substrate and on a silicon substrate manifests itself as a single exponential decay with an average lifetime of 19.8 ns and 16.1 ns respectively. The emission dynamics of the QD monolayer, on the other hand, are strongly affected by the nanogap modes. This coupling manifests itself in the form of enhancements in both emission decay rate (Fig. 4) and photoluminescence intensity (Fig. 5). Coupling the QD monolayer to the nanogap changes the nature of the emission decay dynamics and it is best fit with two decay channels ($I(t) = a_1 e^{-\Gamma_1 t} + a_2 e^{-\Gamma_2 t}$). The fast decay component $\Gamma_1 = \frac{1}{\tau_1}$ is attributed to the coupling between the QDs dipoles and the strongly confined electromagnetic field within the

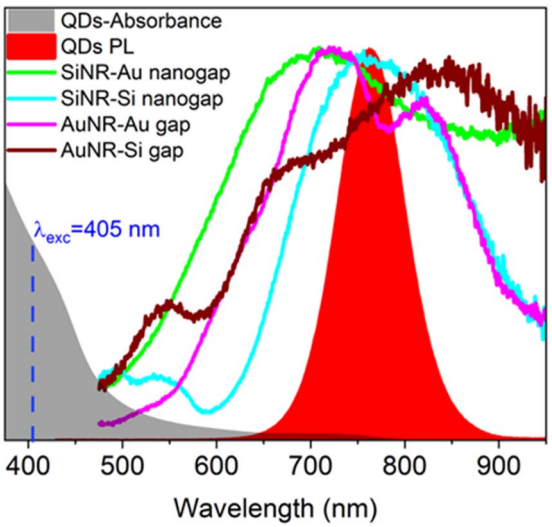

Fig. 3 Absorption and photoluminescence spectrum of CdTe QDs alongside the measured scattering spectra of SiNR–Au, SiNR–Si, AuNR–Au and AuNR–Si nanogaps.

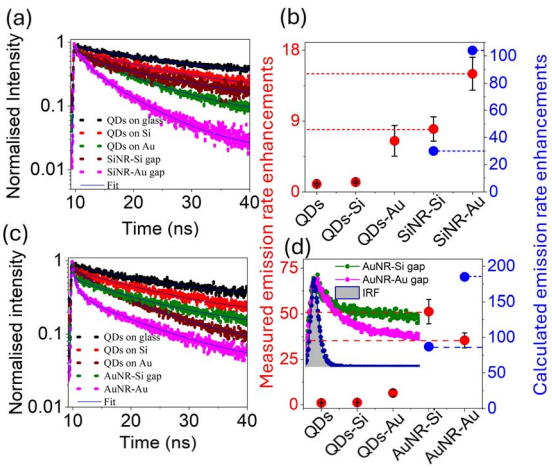

Fig. 4 (a) Photoluminescence decay curves of SiNR–Au and SiNR–Si nanogaps. For comparison the photoluminescence decay curves of CdTe quantum dots on glass, Si substrate and gold film are shown. (b) Comparison between calculated and measured emission rate enhancements of SiNR–Au and SiNR–Si nanogaps at $\lambda = 750$ nm. (c) Photoluminescence decay curves of AuNR–Au and AuNR–Si nanogaps. For comparison the photoluminescence decay curves of CdTe quantum dots on glass, Si substrate and gold film are shown. (d) Comparison between calculated and measured emission rate enhancements of AuNR–Au and AuNR–Si nanogaps at $\lambda = 750$ nm. The inset shows a comparison between the photoluminescence decay curves of AuNR–Au, AuNR–Si nanogaps and the instrument response function (IRF) of the setup.

nanogaps. The slow decay rate component $\Gamma_2 = \frac{1}{\tau_2}$ stems from both QDs weakly coupled to the nanogap field and QDs outside the nanogap region located in the laser excitation region. Here it is worth noting that Γ_1 is strongly dependent on the nature of the nanogap, while Γ_2, associated with QDs weakly coupled to

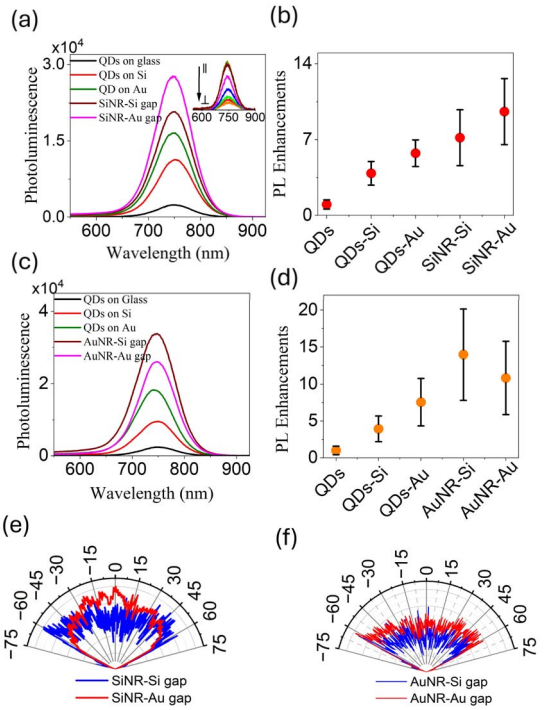

Fig. 5 (a) Photoluminescence spectra of SiNR–Au and SiNR–Si nanogaps. For comparison the photoluminescence spectrum of CdTe quantum dots on glass, Si substrate and gold film are also plotted. The inset shows the polarisation dependence of photoluminescence spectra of SiNR–Au. (b) Measured photoluminescence intensity enhancements of SiNR–Au and SiNR–Si nanogaps. (c) Photoluminescence spectra of AuNR–Au and AuNR–Si nanogaps. For comparison the photoluminescence spectrum of CdTe quantum dots on glass, Si substrate and gold film are shown. (d) Measured photoluminescence intensity enhancements of AuNR–Au and AuNR–Si nanogaps. (e) The measured emission profile of SiNR–Au and SiNR–Si nanogaps at wavelength of $\lambda = 750$ nm. (f) Measured angular emission distribution of AuNR–Au and AuNR–Si nanogaps at wavelength of $\lambda = 750$ nm.

the nanogap field, does not correlate with the nature of the nanogap (see Fig. S9 and Table S1).

The emission rate enhancements from the experimentally fabricated nanogaps (Fig. 4) show a qualitative agreement with the FDTD simulations (Fig. 2). However, the calculated values are consistently higher than the experimentally measured values, with the difference varying from system to system: 4 to 7 times larger for both SiNR based nanogap geometries (SiNR–Si and SiNR–Au), 3 times larger for AuNR–Au, and 1.7 times larger for AuNR–Si nanogaps.

The measured emission rate enhancements are 8 times and 15 times for the purely dielectric SiNR–Si nanogaps and the hybrid SiNR–Au nanogaps and 35 times and 51 times for the purely AuNR–Au nanogaps and the hybrid AuNR–Si nanogaps respectively. These results highlight that hybrid nanogaps outperform their homogeneous equivalent.

Additionally, the experimental emission rate enhancements are larger for AuNR–Si nanogaps than AuNR–Au nanogaps, in contradiction with the FDTD calculations (Fig. 2e and f). This disagreement can be attributed to several factors: (i) whereas

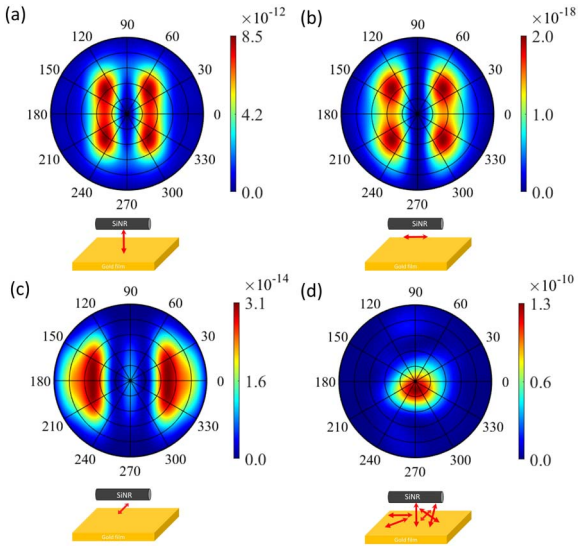

Fig. 6 Calculated emission profile of SiNR–Au nanogap at $\lambda = 750$ nm with (a) a vertical dipole, (b) a horizontal dipole polarised along the long axis of the SiNR, (c) a horizontal dipole polarised along the short axis of the SiNR and (d) for a randomly distribution of dipoles.

the FDTD results in Fig. 2 represent the outcome of the ideal case, where the active monolayer was modelled as a single vertical dipole located at the centre of the emission monolayer and the nanogap, the experimental measurements contain a distribution of randomly oriented dipoles located across the emission monolayer. (ii) Experimental imperfections in the gold film (*e.g.* surface roughness, see Fig. S10) and nanorods (defects in the nanorods facets and edges, see Fig. S1) can adversely affect the nanogap properties.[21,72–76] (iii) for both those systems, the coupling to the nanogap results in a fast component comparable with the system IRF, resulting in the measured enhancements (Fig. 4d) to be limited by the temporal resolution or our set-up, therefore being more representative of a lower-bound rather than absolute emission rate enhancements.

The PL spectra of a QD monolayer complement the emission rate enhancements measurements, showing a clear enhancement in emission intensity when coupled to a nanogap geometry compared to the QD monolayer on a glass substrate, a Si substrate, or a gold film (Fig. 5). These PL intensity enhancements (see Fig. 5b and d) follow the trend observed in the emission decay rate enhancements in Fig. 4b and d, confirming that the observed PL intensity enhancements are due to the coupling between QDs dipoles and nanogap modes. Additionally, it is important to note that the PL intensity enhancements in Fig. 5b and d represent a lower-bound estimate of the intensity enhancements as the number of QDs in the excitation area ($\sim$0.79 μm^2) is 6 to 8 times larger than the QDs in each nanogaps, determined by the cross sectional area of the corresponding nanorod, $\sim$0.14 μm^2 for SiNR and $\sim$0.1 μm^2 for AuNR. Assuming QDs in the nanogaps are equally excited, this difference in the number of QDs contributing to the nanogap signal and the reference results in a further geometrical excitation enhancement factor of 6–8 times for the SiNR-based nanogaps and the AuNR-based nanogaps respectively when normalizing to a QD monolayer. Accordingly, the actual photoluminescence enhancement factor is 40 times and 54 times for the purely dielectric SiNR–Si nanogaps and the hybrid SiNR–Au nanogaps and 85 times and 110 times for the purely gold AuNR–Au nanogaps and for the hybrid AuNR–Si nanogaps respectively. These results highlight that hybrid nanogaps outperform their purely metal and dielectric counterpart.

Moreover, due to the nanorods geometrical factor, the nanogaps are inherently anisotropic, which translates into polarization dependent emission properties. This is clearly demonstrated in the inset of Fig. 5a, where $\parallel$ and $\perp$ represent an emission polarisation parallel and perpendicular to the nanorod long axis respectively. Similar behaviour was observed across all nanogaps geometries.

Finally, it is interesting to compare the emission profile of the experimental nanogaps (Fig. 5e and f) with the ideal case in the simulations (Fig. 2d and f). Contrary to the simulations results, which showed well defined directional emission (Fig. 2d and f), the experimental emission profiles have lost their directionality with an almost uniformly distributed emission over the collection cone ($\theta = 63°$). This discrepancy can be attributed to a combination of the structural imperfections discussed earlier, the random distribution and orientation of emitters across the nanogap region. Due to the large number of QDs inside the nanogap, each emitter has its own emission profile, and the measured emission profile in Fig. 5e and f represents the sum of all possible profiles for these dipoles. This idea is presented in Fig. 6, where we plot the calculated far-field profile of SiNR–Au nanogap for a vertical dipole located at the centre of the QD monolayer (Fig. 6a), a horizontal dipole polarized along the long axis of the SiNR (Fig. 6b), a horizontal dipole polarized along the short axis of the SiNR (Fig. 6c) and a randomly distributed dipoles (Fig. 6d). From this comparison it is apparent that the presence of random distribution of dipoles within the nanogap modifies the emission profile of the nanogap drastically.

Conclusions

In summary, we have demonstrated the hybrid dielectric–metal nanogaps potential for controlling the emission process of quantum emitters, highlighting the superiority of hybrid nanogap architectures over their purely metallic/high refractive index dielectric equivalent for emission control. FDTD modelling revealed that hybrid dielectric–metallic nanogaps offer spontaneous emission rate enhancements over a 100 times, with quantum efficiencies higher than 50%, combined with directional emission compatible with dry microscope objectives (NA < 0.7). This was verified experimentally for both silicon nanorods on gold film (SiNR–Au) and gold nanorods on silicon surface (AuNR–Si), achieving 15 times emission rate enhancement combined with 54 photoluminescence intensity enhancement for SiNR–Au nanogaps, and 51 times emission rate enhancement with 110 times intensity enhancement for AuNR–Si nanogaps. The hybrid structures developed here pave the way for novel applications in low-cost and low-power

consumption ultrafast nanoLEDs for short distance on-chip and chip-to-chip communications.

Conflicts of interest

There are no conflicts to declare.

Data availability

The data supporting this article have been included as part of the SI.

Uniformity study of the CdTe quantum dot monolayer. Structural characterisation of the synthesised Si nanorods. Zeta potential data of the CdTe quantum dots. Darkfield images of the investigated nanogaps. Calculated x–y cut of the electric field distribution (Im(E_z)) at the emission wavelength of the investigated nanogaps. Far-field emission profile of the investigated nanogaps at different wavelength. Calculated emission rate enhancements and quantum yield of the investigated nanogaps as function of the gold/silicon film thickness. Details of the photophysics of the investigated nanogaps. AFM characterisation of of the used gold film. See DOI: **https://doi.org/10.1039/d5ra04583e**.

Acknowledgements

We thank the University of Diyala and Schlumberger the faculty for the future for supporting A. Al-Hamandani to study for a PhD at the University of Hull. Also, we thank the University of Hull and the University of Diyala for the provision of a PhD scholarship for A. Al-Dulami. This work was supported by the EU Horizon 2020 research and innovation programme under grant number 861950, project POSEIDON. We also acknowledge the Viper High Performance Computing facility of the University of Hull and its support team. This research was funded in whole or in part by the Austrian Science Fund (FWF) P33159 and the Austrian Academy of Sciences (ÖAW; grant number 26939). For open access purposes, the author has applied for a CC BY public copyright license to any author accepted manuscript version arising from this submission.

Notes and references

1 M. T. Clarke, F. N. Viscomi, T. W. Chamberlain, N. Hondow, A. M. Adawi, J. Sturge, S. C. Erwin, J. S. G. Bouillard, S. Tamang and G. J. Stasiuk, Synthesis of Super Bright Indium Phosphide Colloidal Quantum Dots through Thermal Diffusion, *Commun. Chem.*, 2019, **2**, 36, DOI: **10.1038/s42004-019-0138-z**.

2 G. E. Khalil, A. M. Adawi, A. M. Fox, A. Iraqi and D. G. Lidzey, Single Molecule Spectroscopy of Red- and Green-Emitting Fluorene-Based Copolymers, *J. Chem. Phys.*, 2009, **130**(4), 2–9, DOI: **10.1063/1.3054142**.

3 M. Pelton, Modified Spontaneous Emission in Nanophotonic Structures, *Nat. Photonics*, 2015, **9**(7), 427–435, DOI: **10.1038/nphoton.2015.103**.

4 S. Noda, M. Fujita and T. Asano, Spontaneous-Emission Control by Photonic Crystals and Nanocavities, *Nat. Photonics*, 2007, **1**, 449–458.

5 S. Noda, Recent Progresses and Future Prospects of Two- and Three-Dimensional Photonic Crystals, *J. Lightwave Technol.*, 2006, **24**(12), 4554–4567.

6 R. Zia, J. A. Schuller, A. Chandran and M. L. Brongersma, Plasmonics: The next Chip-Scale Technology The Development of Chip-Scale Electronics and Photonics Has Led To, *Mater. Today*, 2006, **9**(7), 20–27.

7 K. L. Tsakmakidis, R. W. Boyd, E. Yablonovitch and X. Zhang, Large Spontaneous-Emission Enhancements in Metallic Nanostructures: Towards LEDs Faster than Lasers [Invited], *Opt. Express*, 2016, **24**(16), 17916, DOI: **10.1364/oe.24.017916**.

8 S. A. Haque and J. Nelson, Toward Organic All-Optical Switching, *Science*, 2010, **327**(5972), 1466–1467, DOI: **10.1126/science.1188291**.

9 S. Hooten, N. M. Andrade, M. C. Wu and E. Yablonovitch, Efficient Spontaneous Emission by Metal-Dielectric Antennas; Antenna Purcell Factor Explained, *Opt. Express*, 2021, **29**(14), 22018, DOI: **10.1364/oe.423754**.

10 Y. Kan and S. I. Bozhevolnyi, Advances in Metaphotonics Empowered Single Photon Emission, *Adv. Opt. Mater.*, 2023, **11**(10), 2202759, DOI: **10.1002/adom.202202759**.

11 T. B. Hoang, G. M. Akselrod and M. H. Mikkelsen, Ultrafast Room-Temperature Single Photon Emission from Quantum Dots Coupled to Plasmonic Nanocavities, *Nano Lett.*, 2016, **16**(1), 270–275, DOI: **10.1021/acs.nanolett.5b03724**.

12 B. Yang, G. Chen, A. Ghafoor, Y. Zhang, Y. Zhang, Y. Zhang, Y. Luo, J. Yang, V. Sandoghdar, J. Aizpurua, Z. Dong and J. G. Hou, Sub-Nanometre Resolution in Single-Molecule Photoluminescence Imaging, *Nat. Photonics*, 2020, **14**(11), 693–699, DOI: **10.1038/s41566-020-0677-y**.

13 G. M. Akselrod, C. Argyropoulos, T. B. Hoang, C. Ciracì, C. Fang, J. Huang, D. R. Smith and M. H. Mikkelsen, Probing the Mechanisms of Large Purcell Enhancement in Plasmonic Nanoantennas, *Nat. Photonics*, 2014, **8**, 835.

14 R. Esteban, T. V. Teperik and J. J. Greffet, Optical Patch Antennas for Single Photon Emission Using Surface Plasmon Resonances, *Phys. Rev. Lett.*, 2010, **104**, 026802, DOI: **10.1103/PhysRevLett.104.026802**.

15 A. P. Edwards and A. M. Adawi, Plasmonic Nanogaps for Broadband and Large Spontaneous Emission Rate Enhancement, *J. Appl. Phys.*, 2014, **115**(5), 053101, DOI: **10.1063/1.4864018**.

16 Y. Akahane, T. Asano, B. S. Song and S. Noda, High-Q Photonic Nanocavity in a Two-Dimensional Photonic Crystal, *Nature*, 2003, **425**(6961), 944–947, DOI: **10.1038/nature02063**.

17 A. Adawi, M. Murshidy, P. Fry and D. Lidzey, An Optical Nanocavity Incorporating a Fluorescent Organic Dye Having a High Quality Factor, *ACS Nano*, 2010, **4**(6), 3039–3044, DOI: **10.1021/nn1001479**.

18 S. Haddadi, L. Le-Gratiet, I. Sagnes, F. Raineri, A. Bazin, K. Bencheikh, J. A. Levenson and A. M. Yacomotti, High Quality Beaming and Efficient Free-Space Coupling in L3

Photonic Crystal Active Nanocavities, *Opt. Express*, 2012, **20**(17), 18876, DOI: 10.1364/oe.20.018876.

19 J. Baumberg, J. Aizpurua, M. H. Mikkelsen and D. R. Smith, Extreme Nanophotonics from Ultrathin Metallic Gaps, *Nat. Mater.*, 2019, **18**(7), 668–678, DOI: 10.1038/s41563-019-0290-y.

20 G. C. Li, Q. Zhang, S. A. Maier and D. Lei, Plasmonic Particle-on-Film Nanocavities: A Versatile Platform for Plasmon-Enhanced Spectroscopy and Photochemistry, *Nanophotonics*, 2018, **7**(12), 1865–1889, DOI: 10.1515/nanoph-2018-0162.

21 K. J. Russell, T. Liu, S. Cui and E. L. Hu, Large Spontaneous Emission Enhancement in Plasmonic Nanocavities, *Nat. Photonics*, 2012, **6**, 459–462, DOI: 10.1038/NPHOTON.2012.112.

22 G. Yang, Y. Niu, H. Wei, B. Bai and H. B. Sun, Greatly Amplified Spontaneous Emission of Colloidal Quantum Dots Mediated by a Dielectric-Plasmonic Hybrid Nanoantenna, *Nanophotonics*, 2012, **8**(12), 2313–2319, DOI: 10.1515/nanoph-2019-0332.

23 S. Bidault, M. Mivelle and N. Bonod, Dielectric Nanoantennas to Manipulate Solid-State Light Emission, *J. Appl. Phys.*, 2019, **126**(9), 094104, DOI: 10.1063/1.5108641.

24 R. Regmi, J. Berthelot, P. M. Winkler, M. Mivelle, J. Proust, F. Bedu, I. Ozerov, T. Begou, J. Lumeau, H. Rigneault, M. F. García-Parajó, S. Bidault, J. Wenger and N. Bonod, All-Dielectric Silicon Nanogap Antennas to Enhance the Fluorescence of Single Molecules, *Nano Lett.*, 2016, **16**(8), 5143–5151, DOI: 10.1021/acs.nanolett.6b02076.

25 B. Kalinic, T. Cesca, I. G. Balasa, M. Trevisani, A. Jacassi, S. A. Maier, R. Sapienza and G. Mattei, Quasi-BIC Modes in All-Dielectric Slotted Nanoantennas for Enhanced Er3+ Emission, *ACS Photonics*, 2023, **10**(2), 534–543, DOI: 10.1021/acsphotonics.2c01703.

26 L. Sortino, P. G. Zotev, S. Mignuzzi, J. Cambiasso, D. Schmidt, A. Genco, M. Aßmann, M. Bayer, S. A. Maier, R. Sapienza and A. I. Tartakovskii, Enhanced Light-Matter Interaction in an Atomically Thin Semiconductor Coupled with Dielectric Nano-Antennas, *Nat. Commun.*, 2019, **10**(1), 5119, DOI: 10.1038/s41467-019-12963-3.

27 R. M. Córdova-Castro, B. van Dam, A. Lauri, S. A. Maier, R. Sapienza, Y. De Wilde, I. Izeddin and V. Krachmalnicoff, Single-Emitter Super-Resolved Imaging of Radiative Decay Rate Enhancement in Dielectric Gap Nanoantennas, *Light Sci. Appl.*, 2024, **13**(1), 7, DOI: 10.1038/s41377-023-01349-2.

28 L. Sortino, P. G. Zotev, C. L. Phillips, A. J. Brash, J. Cambiasso, E. Marensi, A. M. Fox, S. A. Maier, R. Sapienza and A. I. Tartakovskii, Bright Single Photon Emitters with Enhanced Quantum Efficiency in a Two-Dimensional Semiconductor Coupled with Dielectric Nano-Antennas, *Nat. Commun.*, 2021, **12**(1), 1–9, DOI: 10.1038/s41467-021-26262-3.

29 C. Vidal, B. Tilmann, S. Tiwari, T. V. Raziman, S. A. Maier, J. Wenger and R. Sapienza, Fluorescence Enhancement in Topologically Optimized Gallium Phosphide All-Dielectric Nanoantennas, *Nano Lett.*, 2024, **24**(8), 2437–2443, DOI: 10.1021/acs.nanolett.3c03773.

30 P. G. Zotev, Y. Wang, L. Sortino, T. Severs Millard, N. Mullin, D. Conteduca, M. Shagar, A. Genco, J. K. Hobbs, T. F. Krauss and A. I. Tartakovskii, Transition Metal Dichalcogenide Dimer Nanoantennas for Tailored Light-Matter Interactions, *ACS Nano*, 2022, **16**(4), 6493–6505, DOI: 10.1021/acsnano.2c00802.

31 A. Barreda, F. Vitale, A. E. Minovich, C. Ronning and I. Staude, A Applications of Hybrid Metal-Dielectric Nanostructures State of the Art, *Adv. Photonics Res.*, 2022, **3**, 2100286.

32 A. Barreda, S. Hell, M. A. Weissflog, A. Minovich, T. Pertsch and I. Staude, Metal, Dielectric and Hybrid Nanoantennas for Enhancing the Emission of Single Quantum Dots: A Comparative Study, *J. Quant. Spectrosc. Radiat. Transfer*, 2021, **276**, 107900, DOI: 10.1016/j.jqsrt.2021.107900.

33 A. L. Holsteen, S. Raza, P. Fan, P. G. Kik and M. L. Brongersma, Purcell Effect for Active Tuning of Light Scattering from Semiconductor Optical Antennas, *Science*, 2017, **358**, 1407–1410, DOI: 10.1017/CBO9781139013475.

34 K. Larsen, D. Austin, I. C. Sandall, D. G. Davies, D. G. Revin, J. W. Cockburn, A. M. Adawi, R. J. Airey, P. W. Fry, M. Hopkinson and L. R. Wilson, Electrical Modulation of the Optical Properties of Mid-Infrared Metamaterials, *Appl. Phys. Lett.*, 2012, **101**(25), 99–102, DOI: 10.1063/1.4772545.

35 H. Sugimoto, R. Imaizumi, T. Hinamoto, T. Kawashima and M. Fujii, Silicon Nanowire on Mirror Nanoantennas: Engineering Hybrid Gap Mode for Light Sources and Sensing Platforms, *ACS Appl. Nano Mater.*, 2020, **3**(7), 7223–7230, DOI: 10.1021/acsanm.0c01559.

36 E. Mohammadi, A. Tittl, K. L. Tsakmakidis, T. V. Raziman and A. G. Curto, Dual Nanoresonators for Ultrasensitive Chiral Detection, *ACS Photonics*, 2021, **8**(6), 1754–1762, DOI: 10.1021/acsphotonics.1c00311.

37 H. Sugimoto and M. Fujii, Broadband Dielectric-Metal Hybrid Nanoantenna: Silicon Nanoparticle on a Mirror, *ACS Photonics*, 2018, **5**(5), 1986–1993, DOI: 10.1021/acsphotonics.7b01461.

38 V. J. Sorger, N. Pholchai, E. Cubukcu, R. F. Oulton, P. Kolchin, C. Borschel, M. Gnauck, C. Ronning and X. Zhang, Strongly Enhanced Molecular Fluorescence inside a Nanoscale Waveguide Gap, *Nano Lett.*, 2011, **11**(11), 4907–4911, DOI: 10.1021/nl202825s.

39 A. Maimaiti, P. P. Patra, S. Jones, T. J. Antosiewicz and R. Verre, Low-Loss Hybrid High-Index Dielectric Particles on a Mirror for Extreme Light Confinement, *Adv. Opt. Mater.*, 2020, **8**(6), 1901820, DOI: 10.1002/adom.201901820.

40 J. H. Kim, H. S. Lee, G. H. An, J. Lee, H. M. Oh, J. Choi and Y. H. Lee, Dielectric Nanowire Hybrids for Plasmon-Enhanced Light-Matter Interaction in 2D Semiconductors, *ACS Nano*, 2020, **14**(9), 11985–11994, DOI: 10.1021/acsnano.0c05158.

41 X. He, S. Liu, S. Li, M. Panmai and S. Lan, Si/Au Hybrid Nanoparticles with Highly Efficient Nonlinear Optical Emission: Implication for Nanoscale White Light Sources, *ACS Appl. Nano Mater.*, 2022, **5**(8), 10676–10685, DOI: 10.1021/acsanm.2c01982.

42 P. A. Dmitriev, E. Lassalle, L. Ding, Z. Pan, D. C. J. Neo, V. Valuckas, R. Paniagua-Dominguez, J. K. W. Yang, H. V. Demir and A. I. Kuznetsov, Hybrid Dielectric-Plasmonic Nanoantenna with Multiresonances for Subwavelength Photon Sources, *ACS Photonics*, 2023, **10**(3), 582–594, DOI: 10.1021/acsphotonics.2c01332.

43 L. Wang, X. Wang, S. Mao, H. Wu, X. Guo, Y. Ji and X. Han, Strongly Enhanced Ultraviolet Emission of an Au@SiO2/ZnO Plasmonic Hybrid Nanostructure, *Nanoscale*, 2016, **8**(7), 4030–4036, DOI: 10.1039/c5nr06153a.

44 Y. Bian and Q. Gong, Tuning the Hybridization of Plasmonic and Coupled Dielectric Nanowire Modes for High-Performance Optical Waveguiding at Sub-Diffraction-Limited Scale, *Sci. Rep.*, 2014, **4**, 6617, DOI: 10.1038/srep06617.

45 J. S. Wang, K. P. Chiu, C. Y. Lin, Y. H. Tsai and C. T. Yuan, Modification of Spontaneous Emission Rates of Self-Assembled CdSe Quantum Dots by Coupling to Hybrid Optical Nanoantennas, *Plasmonics*, 2017, **12**(2), 433–438, DOI: 10.1007/s11468-016-0282-6.

46 G. Decher, Fuzzy Nanoassemblies : Toward Layered Polymeric Multicomposites Published by : American Association for the Advancement of Science Linked References Are Available on JSTOR for This Article : Fuzzy Nanoassemblies : Toward Layered Polymeric Mu Ticom Posites, *Science*, 1997, **277**(5330), 1232–1237.

47 Y. Wang, M. Zhang, Y. Lai and L. Chi, Advanced Colloidal Lithography: From Patterning to Applications, *Nano Today*, 2018, **22**, 36–61, DOI: 10.1016/j.nantod.2018.08.010.

48 M. Li, Y. Li, W. Liu, L. Yue, R. Li, Y. Luo, M. Trevor, B. Jiang, F. Bai, P. Fu, Y. Zhao, C. Shen and J. M. Mbengue, Metal-Assisted Chemical Etching for Designable Monocrystalline Silicon Nanostructure, *Mater. Res. Bull.*, 2016, **76**, 436–449, DOI: 10.1016/j.materresbull.2016.01.006.

49 P. B. Johnson and R. W. Christy, Optical Constants of the Noble Metals, *Phys. Rev. B*, 1972, **6**(12), 4370–4379, DOI: 10.1103/PhysRevB.6.4370.

50 E. D. Palik, *Handbook of Optical Constants of Solids*, Elsevier Science, 1998.

51 T. Bartschmid, A. Farhadi, M. E. Musso, E. S. A. Goerlitzer, N. Vogel and G. R. Bourret, Self-Assembled Au Nanoparticle Monolayers on Silicon in Two- and Three-Dimensions for Surface-Enhanced Raman Scattering Sensing, *ACS Appl. Nano Mater.*, 2022, **5**, 11839–11851, DOI: 10.1021/acsanm.2c01904.

52 T. Bartschmid, F. J. Wendisch, A. Farhadi and G. R. Bourret, Recent Advances in Structuring and Patterning Silicon Nanowire Arrays for Engineering Light Absorption in Three Dimensions, *ACS Appl. Energy Mater.*, 2021, **5**, 5307–5317, DOI: 10.1021/acsaem.1c02683.

53 M. Rey, F. J. Wendisch, E. S. Aaron Goerlitzer, J. S. Julia Tang, R. S. Bader, G. R. Bourret and N. Vogel, Anisotropic Silicon Nanowire Arrays Fabricated by Colloidal Lithography, *Nanoscale Adv.*, 2021, **3**(12), 3634–3642, DOI: 10.1039/d1na00259g.

54 F. J. Wendisch, M. Abazari, H. Mahdavi, M. Rey, N. Vogel, M. Musso, O. Diwald and G. R. Bourret, Morphology-Graded Silicon Nanowire Arrays via Chemical Etching: Engineering Optical Properties at the Nanoscale and Macroscale, *ACS Appl. Mater. Interfaces*, 2020, **12**(11), 13140–13147, DOI: 10.1021/acsami.9b21466.

55 F. J. Wendisch, M. Rey, N. Vogel and G. R. Bourret, Large-Scale Synthesis of Highly Uniform Silicon Nanowire Arrays Using Metal-Assisted Chemical Etching, *Chem. Mater.*, 2020, **32**(21), 9425–9434, DOI: 10.1021/acs.chemmater.0c03593.

56 Z. Huang, N. Geyer, P. Werner, J. Boor and U. Gosele, Metal-Assisted Chemical Etching of Silicon: A Review, *Adv. Mater.*, 2011, **23**, 285–308, DOI: 10.1002/adma.201001784.

57 J. Menath, J. Eatson, R. Brilmayer, A. Andrieu-brunsen, D. M. A. Buzza and N. Vogel, De Fi Ned Core – Shell Particles as the Key to Complex Interfacial Self-Assembly, *Proc. Natl. Acad. Sci. U. S. A.*, 2021, **118**, e2113394118, DOI: 10.1073/pnas.2113394118.

58 M. Rey, M. Á. Fernández-Rodríguez, M. Steinacher, L. Scheidegger, K. Geisel, W. Richtering, T. M. Squires and L. Isa, Isostructural Solid-Solid Phase Transition in Monolayers of Soft Core-Shell Particles at Fluid Interfaces: Structure and Mechanics, *Soft Matter*, 2016, **12**(15), 3545–3557, DOI: 10.1039/c5sm03062e.

59 J. S. J. Tang, R. S. Bader, E. S. A. Goerlitzer, J. F. Wendisch, G. R. Bourret, M. Rey and N. Vogel, Surface Patterning with SiO2@PNiPAm Core-Shell Particles, *ACS Omega*, 2018, **3**(9), 12089–12098, DOI: 10.1021/acsomega.8b01985.

60 A. Farhadi, T. Bartschmid and G. R. Bourret, Dewetting-Assisted Patterning: A Lithography-Free Route to Synthesize Black and Colored Silicon, *ACS Appl. Mater. Interfaces*, 2023, **15**(37), 44087–44096, DOI: 10.1021/acsami.3c08533.

61 B. Y. Wen, J. Y. Wang, T. L. Shen, Z. W. Zhu, P. C. Guan, J. S. Lin, W. Peng, W. W. Cai, H. Jin, Q. C. Xu, Z. L. Yang, Z. Q. Tian and J. F. Li, Manipulating the Light-Matter Interactions in Plasmonic Nanocavities at 1 Nm Spatial Resolution, *Light Sci. Appl.*, 2022, **11**(1), 235, DOI: 10.1038/s41377-022-00918-1.

62 S. Y. Bang, Y.-H. Suh, X.-B. Fan, D.-W. Shin, S. Lee, H. W. Choi, T. H. Lee, J. Yang, S. Zhan, W. Harden-Chaters, C. Samarakoon, L. G. Occhipinti, S. D. Han, S.-M. Jung and J. M. Kim, Technology Progress on Quantum Dot Light-Emitting Diodes for next-Generation Displays, *Nanoscale Horiz.*, 2021, **6**(2), 68–77, DOI: 10.1039/D0NH00556H.

63 D. Pagnotto, A. Muravitskaya, D. Benoit, J.-S. Bouillard and A. M. Adawi, Stark Effect Control of the Scattering Properties of Plasmonic Nanogaps Containing an Organic Semiconductor, *ACS Appl. Opt. Mater.*, 2023, **1**(1), 500–506, DOI: 10.1021/acsaom.2c00135.

64 A. O. Hamza, A. Al-Dulaimi, J. S. G. Bouillard and A. M. Adawi, Long-Range and High-Efficiency Plasmon-Assisted Förster Resonance Energy Transfer, *J. Phys. Chem. C*, 2023, **127**(44), 21611–21616, DOI: 10.1021/acs.jpcc.3c04281.

65 V. J. Sorger, N. Pholchai, E. Cubukcu, R. F. Oulton, P. Kolchin, C. Borschel, M. Gnauck, C. Ronning and

X. Zhang, Strongly Enhanced Molecular Fluorescence inside a Nanoscale Waveguide Gap, *Nano Lett.*, 2011, **11**(11), 4907–4911, DOI: **10.1021/nl202825s**.

66 A. Rose, T. B. Hoang, F. McGuire, J. J. Mock, C. Ciracì, D. R. Smith and M. H. Mikkelsen, Control of Radiative Processes Using Tunable Plasmonic Nanopatch Antennas, *Nano Lett.*, 2014, **14**(8), 4797–4802, DOI: **10.1021/nl501976f**.

67 L. Novotny and B. Hecht, *Principles of Nano-Optics*, Cambridge University Press, Cambridge, 2012, DOI: **10.1017/CBO9780511794193**.

68 F. Le, N. Z. Lwin, J. M. Steele, M. Käll, N. J. Halas and P. Nordlander, Plasmons in the Metallic Nanoparticle-Film System as a Tunable Impurity Problem, *Nano Lett.*, 2005, **5**(10), 2009–2013, DOI: **10.1021/nl0515100**.

69 P. Nordlander and E. Prodan, Plasmon Hybridization in Nanoparticles near Metallic Surfaces, *Nano Lett.*, 2004, **4**(11), 2209–2213, DOI: **10.1021/nl0486160**.

70 R. Chikkaraddy and J. J. Baumberg, Accessing Plasmonic Hotspots Using Nanoparticle-on-Foil Constructs, *ACS Photonics*, 2021, **8**(9), 2811–2817, DOI: **10.1021/acsphotonics.1c01048**.

71 R. E. Armstrong, J. C. Van Liempt and P. Zijlstra, Effect of Film Thickness on the Far- A Nd Near-Field Optical Response of Nanoparticle-on-Film Systems, *J. Phys. Chem. C*, 2019, **123**(42), 25801–25808, DOI: **10.1021/acs.jpcc.9b06592**.

72 C. Ciracì, F. Vidal-Codina, D. Yoo, J. Peraire, S. H. Oh and D. R. Smith, Impact of Surface Roughness in Nanogap Plasmonic Systems, *ACS Photonics*, 2020, **7**(4), 908–913, DOI: **10.1021/acsphotonics.0c00099**.

73 X. You, W. Peng, J. X. He, J. S. Lin, X. Q. Zong, N. Zhao, J. L. Yang, M. De Li, Y. J. Zhang, J. Yi, H. Jin, Z. Q. Tian and J. F. Li, Inhomogeneity of Fluorescence Lifetime and Intensity in a Plasmonic Nanocavity, *Nano Today*, 2022, **45**, 101548, DOI: **10.1016/j.nantod.2022.101548**.

74 E. Elliott, K. Bedingfield, J. Huang, S. Hu, B. D. Nijs, A. Demetriadou and J. J. Baumberg, Fingerprinting the Hidden Facets of Plasmonic Nanocavities, *ACS Photonics*, 2022, **9**, 2643–2651, DOI: **10.1021/acsphotonics.2c00116**.

75 F. Benz, R. Chikkaraddy, A. Salmon, H. Ohadi, B. De Nijs, J. Mertens, C. Carnegie, R. W. Bowman and J. J. Baumberg, SERS of Individual Nanoparticles on a Mirror: Size Does Matter, but so Does Shape, *J. Phys. Chem. Lett.*, 2016, **7**(12), 2264–2269, DOI: **10.1021/acs.jpclett.6b00986**.

76 G. M. Akselrod, C. Argyropoulos, T. B. Hoang, C. Ciracì, C. Fang, J. Huang, D. R. Smith and M. H. Mikkelsen, Probing the Mechanisms of Large Purcell Enhancement in Plasmonic Nanoantennas, *Nat. Photonics*, 2014, **8**(11), 835–840, DOI: **10.1038/nphoton.2014.228**.